Geophysical Research Letters

Supporting Information for

Matrix Diffusion as a Mechanism Contributing to Fractal Stream Chemistry and Long-Tailed Transit Time Distributions

Harihar Rajaram[1]

[1]Department of Environmental Health and Engineering, Johns Hopkins University

Contents of this file

Introduction

Sections S.1 and S.2 provide detailed mathematical steps involved in the derivation of the key results pertaining to the stream concentration power spectrum (Equations (11-12) and (15)). Section S.2 includes a generalization of Equation (15) for the case of a gamma advective travel time distribution. Section S.3 provides a review of Laplace transforms (from previous literature), which are involved in the representation of the Green's function $g\left(T_a;t-T_a\right)$ needed for the evaluation of the solute TTD (Equation (18)) for finite matrix widths. Although the integral (Equation (18)) for the solute TTD can be evaluated exactly only by numerical integration, analytical approximations can be derived for infinite matrix width in three different dimensionless time regimes – these analytical approximations are presented in Section S.4, and provide additional insights into the power-law behavior of solute TTDs. Calculations of the stream concentration power spectrum for Lower Hafren, based on alternative parameter sets and an alternative precipitation concentration spectrum are presented in Section S.5.

S.1 Detailed Derivation of the Fourier Transform Solution for $\tilde{C}_f$ (Equations 11-12 in the manuscript)

The transport equation in the fracture is given by:

$$\frac{\partial C_f}{\partial t}+\frac{\partial C_f}{\partial \tau_a}=\frac{2\phi_m D_e}{b}\left.\frac{\partial C_m}{\partial z}\right|_{\tau_a, z=0, t} \qquad \text{(S1) (Equation 5 in the manuscript)}$$

The inflow boundary condition at the entrance to the streamline ($\tau_a = 0$) is:

$$C_f(\tau_a = 0, t; I_{T_a}) = C_i(t) \qquad \text{(S2) (Equation 6 in the manuscript)}$$

The right-hand side of (S1) may be evaluated by considering the diffusion equation in the rock matrix:

$$\left(\phi_m + \rho_b K_d\right)\frac{\partial C_m}{\partial t} - \phi_m D_e \frac{\partial^2 C_m}{\partial z^2} = 0 \qquad \text{(S3) (Equation 2 in the manuscript)}$$

Boundary conditions for (S3) are:

$$C_m(\tau_a, z = 0, t; I_{T_a}) = C_f(\tau_a, t; I_{T_a}), \quad \frac{\partial C_m}{\partial z}(\tau_a, z = B, t; I_{T_a}) = 0 \text{ (S4) (Equation 3 in the manuscript,}$$

with τ_a in place of *s*)

The notation $\tilde{C}_i(\omega), \tilde{C}_o(\omega), \tilde{C}_f(\tau_a, \omega; I_{T_a})$ and $\tilde{C}_m(\tau_a, z, \omega; I_{T_a})$ is used for the Fourier transforms of $C_i(t), C_o(t), C_f(\tau_a, t; I_{T_a})$ and $C_m(\tau_a, z, t; I_{T_a})$ respectively, with ω denoting the angular frequency.

The first step is to take the Fourier Transform of the matrix diffusion equation (S3) and boundary conditions (S4), which yields (S5) and (S6):

$$i\omega\tilde{C}_m - \frac{D_e}{R}\frac{d^2\tilde{C}_m}{dz^2} = 0 \qquad \text{(S5)}$$

where $R = (1 + \rho_b K_d / \phi_m)$ is the retardation factor in the matrix and $i = \sqrt{-1}$.

$$\tilde{C}_m(\tau_a, z=0, \omega; I_{T_a}) = \tilde{C}_f(\tau_a, \omega; I_{T_a}), \quad \frac{d\tilde{C}_m}{dz}(\tau_a, z=B, \omega; I_{T_a}) = 0 \quad \text{(S6)}$$

Equations (S5-S6) are then readily solved to obtain $\tilde{C}_m$ in terms of $\tilde{C}_f$:

$$\tilde{C}_m = \tilde{C}_f \left(\frac{e^{-\sqrt{i}uz} + e^{\sqrt{i}u(z-2B)}}{1 + e^{-2\sqrt{i}uB}} \right), \text{ where } u = \sqrt{\frac{\omega R}{D_e}} \quad \text{(S7)}$$

The Fourier transform of (S1) is:

$$i\omega\tilde{C}_f + \frac{d\tilde{C}_f}{d\tau_a} = \frac{2\phi_m D_e}{b} \left. \frac{\partial \tilde{C}_m}{\partial z} \right|_{\tau_a, z=0, \omega} \quad \text{(S8)}$$

The right hand side of (S8) involves the derivative of $\tilde{C}_m$ at the fracture-matrix interface ($z = 0$),

which can be obtained from (S7):

$$\left. \frac{\partial \tilde{C}_m}{\partial z} \right|_{\tau_a, z=0, \omega} = \tilde{C}_f(\tau_a, \omega) \left(-\sqrt{i}u + \frac{2\sqrt{i}u}{1 + e^{2\sqrt{i}uB}} \right) \quad \text{(S9)}$$

Using (S9) in (S8) yields the following first-order ordinary differential equation for $\tilde{C}_f$:

$$i\omega\tilde{C}_f + \frac{d\tilde{C}_f}{d\tau_a} = \frac{2\phi_m D_e}{b} \tilde{C}_f \left(-\sqrt{i}u + \frac{2\sqrt{i}u}{1 + e^{2\sqrt{i}uB}} \right) \quad \text{(S10)}$$

Equation (S10) can be rewritten as:

$$\frac{d\tilde{C}_f}{d\tau_a} + \left(i\omega + \frac{2\phi_m \sqrt{RD_e\omega}}{b}\sqrt{i} - \frac{\frac{4\phi_m \sqrt{RD_e\omega}}{b}\sqrt{i}}{\left(1 + \exp\left(2\sqrt{\frac{R\omega}{D_e}}B\sqrt{i}\right)\right)} \right) \tilde{C}_f = 0 \quad \text{(S11)}$$

With $k(\omega) = i\omega + \frac{2\phi_m \sqrt{RD_e\omega}}{b}\sqrt{i} - \frac{\frac{4\phi_m \sqrt{RD_e\omega}}{b}\sqrt{i}}{\left(1 + \exp\left(2\sqrt{\frac{R\omega}{D_e}}B\sqrt{i}\right)\right)}$, (Equation 11 in the manuscript)

the solution for $\tilde{C}_f$ is obtained in compact form as:

$$\tilde{C}_f(T_a,\omega;I_{T_a}) = \tilde{C}_i(\omega)\exp\{-k(\omega)T_a\} \quad \text{(S12) (Equation 12 in manuscript)}$$

S.2 Detailed Derivation of the Power Spectrum of Stream Concentration Variations $S_{C_oC_o}$ or catchment spectral filter $S_{C_oC_o}/S_{C_iC_i}$ (Equation 15 in the manuscript)

The Fourier transform of the stream (outflow) concentration, $\tilde{C}_o(\omega)$, can be obtained starting from Equations (13) and (8) in the manuscript:

$$\tilde{C}_o(\omega) = \tilde{C}_i(\omega)\int_0^\infty \exp\{-k(\omega)T_a\}P(T_a)dT_a \quad \text{(S13) (Equation 13 in manuscript)}$$

$$P(T_a) = \frac{1}{\overline{T}_a}\exp\left(-\frac{T_a}{\overline{T}_a}\right) \qquad \text{(S14) (Equation 8 in the manuscript)}$$

(S14) is the exponential advective travel time distribution with mean advective travel time $\overline{T}_a$.

Using (S14), the integral in (S13) evaluates to:

$$\int_0^\infty \exp\{-k(\omega)T_a\}P(T_a)dT_a = \frac{1}{1+k(\omega)\overline{T}_a} \qquad \text{(S15)}$$

To proceed further, I start from the denominator:

$$1+k(\omega)\overline{T}_a = 1+\left(i\omega+\frac{2\phi_m\sqrt{RD_e\omega}}{b}\sqrt{i}-\frac{\frac{4\phi_m\sqrt{RD_e\omega}}{b}\sqrt{i}}{\left(1+\exp\left(2\sqrt{\frac{R\omega}{D_e}}B\sqrt{i}\right)\right)}\right)\overline{T}_a \quad \text{(S16)}$$

To evaluate (S16), first note that

$$1+\exp\left(2\sqrt{\frac{R\omega}{D_e}}B\sqrt{i}\right) = 1+\exp\left(2\sqrt{\frac{R\omega}{D_e}}B\frac{1+i}{\sqrt{2}}\right) = 1+\exp\left(\sqrt{\frac{2R\omega}{D_e}}B\right)\left(\cos\left(\sqrt{\frac{2R\omega}{D_e}}B\right)+i\sin\left(\sqrt{\frac{2R\omega}{D_e}}B\right)\right)$$

Now, let

82 $$m = 1 + \exp\left(\sqrt{\frac{2R\omega}{D_e}}B\right)\cos\left(\sqrt{\frac{2R\omega}{D_e}}B\right), n = \exp\left(\sqrt{\frac{2R\omega}{D_e}}B\right)\sin\left(\sqrt{\frac{2R\omega}{D_e}}B\right)$$

83 Thus, $$1 + k(\omega)\overline{T}_a = 1 + \left(i\omega + \frac{2\phi_m\sqrt{RD_e\omega}}{b}\frac{1+i}{\sqrt{2}} - \frac{4\phi_m\sqrt{RD_e\omega}}{b}\frac{1+i}{\sqrt{2}}\frac{m-in}{m^2+n^2}\right)\overline{T}_a \qquad \text{(S17)}$$

84 The right side of (S17) can be rewritten after separating the real and imaginary parts, as:

85 $$\left(1 + \frac{\sqrt{2RD_e\omega}}{b}\phi_m\overline{T}_a\left(1 - \frac{2(m+n)}{m^2+n^2}\right)\right) + i\left(\omega\overline{T}_a + \frac{\sqrt{2RD_e\omega}}{b}\phi_m\overline{T}_a\left(1 - \frac{2(m-n)}{m^2+n^2}\right)\right)$$

86 Now, let $M = 1 - \frac{2(m+n)}{m^2+n^2}, N = 1 - \frac{2(m-n)}{m^2+n^2}, A = \frac{\phi_m\sqrt{RD_e\overline{T}_a}}{b}$.

87 We can thus write:

88 $$\frac{1}{1 + k(\omega)\overline{T}_a} = \frac{1}{\left(1 + \sqrt{2}AM\sqrt{\omega\overline{T}_a}\right) + i\left(\omega\overline{T}_a + \sqrt{2}AN\sqrt{\omega\overline{T}_a}\right)} \qquad \text{(S18)}$$

89 Finally, $S_{C_oC_o} / S_{C_iC_i}$ is obtained by evaluating the integral in Equation (14) of the manuscript,

$$\left|\int_0^\infty \exp\{-k(\omega)T_a\}P(T_a)\,dT_a\right|^2 = \left|\frac{1}{1 + k(\omega)\overline{T}_a}\right|^2 \qquad \text{(S19)}$$

90

$$= \frac{1}{1 + 2\sqrt{2}AM\sqrt{\omega\overline{T}_a} + 2A^2(M^2+N^2)\omega\overline{T}_a + 2\sqrt{2}AN\left(\omega\overline{T}_a\right)^{3/2} + \omega^2\overline{T}_a^{\,2}}$$

91

92 Equation (S19) leads to the power spectrum of stream concentration variations as Equation (15)

93 in the manuscript.

94 A simpler form of (S19) can be derived for the simpler special case of $B \to \infty$. For this case, the

95 boundary condition at $z = B$ in (S4) is replaced with the requirement that $\tilde{C}_m$ remains bounded.

96 This leads to a simpler expression for $\tilde{C}_m$:

$$\tilde{C}_m = \tilde{C}_f e^{-\sqrt{i}uz} \qquad \text{(S20)}$$

The simpler form of (S11) for this case is:

$$\frac{d\tilde{C}_f}{d\tau_a} + \left(i\omega + \frac{2\phi_m \sqrt{RD_e\omega}}{b}\sqrt{i} \right)\tilde{C}_f = 0 \qquad \text{(S21)}$$

The corresponding simpler form of (S17) is:

$$1 + k(\omega)\overline{T}_a = \left(1 + \frac{\sqrt{2RD_e\omega}}{b}\phi_m \overline{T}_a \right) + i\left(\omega\overline{T}_a + \frac{\sqrt{2RD_e\omega}}{b}\phi_m \overline{T}_a \right) \qquad \text{(S22)}$$

The spectral filter $S_{C_oC_o} / S_{C_iC_i}$ is then obtained as:

$$\left| \frac{1}{1 + k(\omega)\overline{T}_a} \right|^2 = \frac{1}{1 + 2\sqrt{2}A\sqrt{\omega\overline{T}_a} + 4A^2\omega\overline{T}_a + 2\sqrt{2}A\left(\omega\overline{T}_a\right)^{3/2} + \omega^2\overline{T}_a^{\,2}} \qquad \text{(S23)}$$

It is readily verified that (S19) reduces to (S23) when $B \to \infty$, in which case $M, N \to 1$.

In Dupuit flow systems with significant water table relief (i.e. significant increase in saturated thickness *H* from stream to divide), or in the case of deep-circulating groundwater flow, the exponential distribution is not a suitable model for the advective travel time distribution. A gamma distribution (especially with $\alpha < 1$), which has two parameters, provides a more flexible model of the advective travel time distribution in such cases. Equation (14) in the manuscript can be employed with any advective travel time distribution. Below, I present the spectral ratio $S_{C_oC_o} / S_{C_iC_i}$ for a gamma advective travel time distribution (rewritten in terms of the mean advective travel time $\overline{T}_a$):

$$P(T_a) = \frac{\alpha^\alpha}{\Gamma(\alpha)\overline{T}_a}\left(\frac{T_a}{\overline{T}_a} \right)^{\alpha-1} \exp\left(-\alpha\frac{T_a}{\overline{T}_a} \right) \qquad \text{(S24)}$$

114 Using (S24) in Equation (14) of the manuscript, the spectral ratio $S_{C_oC_o} / S_{C_iC_i}$ for a gamma

115 advective travel time distribution is obtained as:

$$\left|\int_0^\infty \exp\{-k(\omega)T_a\}P(T_a)\,dT_a\right|^2 = \left|\frac{\alpha^\alpha}{\left(\alpha + k(\omega)\overline{T}_a\right)^\alpha}\right|^2 =$$

116 $$\frac{\alpha^{2\alpha}}{\left(\alpha^2 + 2\sqrt{2}AM\alpha\sqrt{\omega\overline{T}_a} + 2A^2\left(M^2+N^2\right)\omega\overline{T}_a + 2\sqrt{2}AN\left(\omega\overline{T}_a\right)^{3/2} + \omega^2\overline{T}_a^2\right)^\alpha} \quad \text{(S25)}$$

117 Equation (S25) shows that matrix diffusion combined with a gamma distributed advective travel

118 times across streamlines leads to a richer variety of power-law exponents in stream concentration

119 spectra. For $\alpha = 1$, (S25) reduces to (S19). For strong matrix diffusion (A>>1), the third term in

120 the denominator dominates and the spectral ratio behaves as $1/\omega^\alpha$ for a large frequency range,

121 rather than $1/\omega$ as in (S19 or Equation 15 in the manuscript). For pure advection $(A \to 0)$, the

122 spectral filter reduces to $1/(1+\omega^2\beta^2)^\alpha$, where $\beta = \overline{T}_a / \alpha$; which is consistent with that of the

123 gamma distribution and behaves as $1/\omega^{2\alpha}$ at high frequencies. In general, when matrix diffusion

124 is strong, the spectral ratio behaves as $1/\omega^\alpha$, rather than the $1/\omega^{2\alpha}$ behavior of the

125 corresponding advective travel time distribution, i.e. the power-law exponent of the advective

126 travel time power spectrum is halved as a result of matrix diffusion.

127 **S.3 Review of the Laplace Transform Solutions to (S1) - (S4), relevant to the catchment**

128 **solute TTD *h(t)* (Equation 18 in the manuscript)**

129 Laplace transform solutions for transport with matrix diffusion in fractured rock date back to

130 Grisak and Pickens (1980), Tang et al. (1981) and Maloszewski and Zuber (1985). For

131 completeness, I present the specific forms of the Laplace transforms used in the manuscript here.

I use the following notation to denote a Laplace transform $\hat{f}(s)$ of a function $f(t)$ and the corresponding inverse transform, where t denotes time and s is the Laplace transform variable:

$$\mathcal{L}\{f(t)\}(s) = \hat{f}(s) = \int_0^\infty e^{-st} f(t)dt, \quad \mathcal{L}^{-1}\left\{\hat{f}(s)\right\}(t) = f(t)$$

The Laplace transform of the fracture concentration at the end of a streamline is defined as:

$$\mathcal{L}\left\{C_f(T_a, t; I_{T_a})\right\}(s) = \hat{C}_f(T_a, s; I_{T_a}) \quad \text{(S24)}$$

The corresponding inverse Laplace transform is defined by:

$$\mathcal{L}^{-1}\left\{\hat{C}_f(T_a, s; I_{T_a})\right\}(t) = C_f(T_a, t; I_{T_a}) \quad \text{(S25)}$$

For a Dirac Delta input function, i.e. $C_i(t) = \delta(t)$, solving (S1) - (S4) using Laplace transforms yields:

$$\hat{C}_f(T_a, s; I_{T_a}) = \exp\left(-\left(s + 2a\sqrt{s}\tanh\left(\sqrt{\frac{Rs}{D_e}}B\right)\right)T_a\right) \quad \text{(S26)}$$

where $a = \phi_m\sqrt{RD_e}/b$.

The corresponding inverse Laplace transform is:

$$C_f(T_a, t; I_{T_a}) = H(t - T_a)\,\mathcal{L}^{-1}\left\{\exp\left(-2a\sqrt{s}\tanh\left(\sqrt{\frac{Rs}{D_e}}B\right)T_a\right)\right\}(t - T_a) \quad \text{(S27)}$$

where $H(t - T_a)$ is the Heaviside function (0 for $t \le T_a$ and 1 for $t > T_a$). Thus, if the Green's function (solution for a Dirac delta input) for the coupled equations (S1-S4) is denoted as $H(t - T_a)g(T_a; t - T_a)$, the function $g(T_a; t - T_a)$ is defined as:

$$g(T_a; t - T_a) = \mathcal{L}^{-1}\left\{\exp\left(-2a\sqrt{s}\tanh\left(\sqrt{\frac{Rs}{D_e}}B\right)T_a\right)\right\}(t - T_a) \quad \text{(S28)}$$

For $B \to \infty$, the tanh term in (S28) becomes 1 and the inverse Laplace transform $\mathcal{L}^{-1}\left\{\exp\left(-2a\sqrt{s}T_a\right)\right\}\left(t-T_a\right)$ is obtained analytically (Maloszewski and Zuber, 1985) to yield:

$$g\left(T_a;t-T_a\right)=\frac{aT_a}{\sqrt{\pi}\left(t-T_a\right)^{3/2}}\exp\left(-\frac{a^2T_a^2}{\left(t-T_a\right)}\right) \quad \text{(S29) (Equation 17 in the manuscript)}$$

For finite *B*, the inverse Laplace transform can be written in an integral form (Maloszewski and Zuber, 1985), but is easier to evaluate by numerical inversion of (S28). I used a numerical inversion to evaluate $g\left(T_a;t-T_a\right)$ in (18) for cases with finite matrix width. The MATLAB function "talbot_inversion" (McClure, 2020) was used for numerical Laplace transform inversion. The implementation of the inversion algorithm was verified by computing $\mathcal{L}^{-1}\left\{\exp\left(-2a\sqrt{s}T_a\right)\right\}\left(t-T_a\right)$ numerically and verifying that it matches the analytical form (S29).

S.4. Non-dimensionalization and Approximate Analytical Forms for the solute TTD $h(t)$ with Exponential and Gamma Advective Travel Time Distributions $P(T_a)$ for infinite matrix widths ($B/\sqrt{De\overline{T}_a}$ >>1)

For infinite matrix widths, the general expression (18) for h(t) can be non-dimensionalized and written in terms of dimensionless total $\left(t^*=t/\overline{T_a}\right)$ and advective $\left(T_a^*=T_a/\overline{T_a}\right)$ travel times as:

$$h\left(t^*\right)\overline{T_a}=\int_0^{t^*}\frac{AT_a^*}{\sqrt{\pi}\left(t^*-T_a^*\right)^{3/2}}\exp\left(-\frac{A^2T_a^{*2}}{\left(t^*-T_a^*\right)}\right)\left(P\left(T_a^*\right)\overline{T_a}\right)dT_a^* \qquad \text{(S30)}$$

Note that $h\left(t^*\right)\overline{T_a}$ is the dimensionless solute TTD and $P\left(T_a^*\right)\overline{T_a}$ is the dimensionless advective travel time distribution. Also note that $A=\phi_m\sqrt{RD_e\overline{T}_a}/b=a\sqrt{\overline{T_a}}$, as defined in Equation (16) in the main manuscript. For exponential and gamma advective travel time distributions, the advective travel time distributions are rewritten in dimensionless form below:

Exponential: $$P\left(T_a^*\right)\overline{T_a} = \exp\left(-T_a^*\right) \quad \text{(S31)}$$

Gamma: $$P\left(T_a^*\right)\overline{T_a} = \frac{\alpha^\alpha}{\Gamma(\alpha)}\left(T_a^*\right)^{\alpha-1}\exp\left(-\alpha T_a^*\right) \quad \text{(S32)}$$

Numerical integration of (S30) was performed using the MATLAB function "integral" to obtain the exact dimensionless solute TTD.

There are three dimensionless time regimes in which simpler approximations to (S30) can be developed.

VERY EARLY TIME: As noted in the main manuscript, for very early times ($t^* << 1$), $h\left(t^*\right)\overline{T_a} \to P\left(t^*\right)\overline{T_a}$ for any form of the advective travel time distribution, because $g\left(T_a; t - T_a\right) \to \delta\left(t - T_a\right)$ at short times $(t, T_a \to 0)$. In other words, the solute TTD approaches the advective travel time distribution at very early times. The behavior is confirmed in Figure S1.

ANALYTICAL APPROXIMATION FOR $t^* > 1/A$: Approximate analytical forms of (S30) can be obtained after change of variables and asymptotic approximation of the resulting integral for $t^* > 1/A$ (Hyman et al. 2019):

Exponential: $$h\left(t^*\right)\overline{T_a} \approx \frac{1}{4A^2}\left(\frac{2A}{\sqrt{\pi t^*}} - \exp\left(\frac{t^*}{4A^2}\right)\operatorname{erfc}\left(\frac{\sqrt{t^*}}{2A}\right)\right) \quad \text{(S33)}$$

Gamma: $$h\left(t^*\right)\overline{T_a} \approx \left(\frac{\alpha}{2}\right)^{\alpha+1}\frac{\left(t^*\right)^{-1+\frac{\alpha}{2}}U\left(\frac{1+\alpha}{2}, \frac{1}{2}, \frac{\alpha^2 t^*}{4A^2}\right)}{A^\alpha\sqrt{\pi}} \quad \text{(S34)}$$

where $U(.,.,.)$ is the confluent hypergeometric function of the second kind (Weisstein, 2021), also known as the confluent hypergeometric Kummer U function. It should also be noted that (S33) is essentially a special case of (S34) for $\alpha = 1$, in as much as the exponential distribution is a special case of the gamma distribution for $\alpha = 1$.

Figure S1 shows comparisons between the exact $h\left(t^*\right)\overline{T_a}$ obtained by numerical integration of (S30) and analytical approximations (S33) and (S44). Figure S1 confirms that (S33) and (S34) are excellent approximations to the numerical integral of (S30) for $t^* > 1/A$.

The expressions (S33) and (S34) can be further approximated in intermediate and late time regimes.

INTERMEDIATE-TIME ($1/A < t^* < 4A^2/\alpha^2$) POWER LAW REGIME: An intermediate power-law regime prevails in the dimensionless time range $1/A < t^* < 4A^2/\alpha^2$ (note that this dimensionless time range may not exist for small values of A and larger values of α). This power-law regime is most clearly evident for $A = 10$ in Figure S1, but also for $A = 5$ and $\alpha = 1$, 0.7. From a MacLaurin series expansion of (S34), this power-law regime can be identified as

$$h\left(t^*\right)\overline{T_a} \approx \frac{\left(\alpha/2\right)^{\alpha+1}}{A^{\alpha}\Gamma\left(1+\frac{\alpha}{2}\right)}\left(t^*\right)^{-1+\frac{\alpha}{2}} \qquad \text{(S35)}$$

Equation (S35) is not plotted in Figure S1 to keep it from getting too crowded. Figure S2 shows a comparison between (S35) and (S30) for different values of α and A, and confirms its validity, especially for larger values of A and smaller values of α.

LATE-TIME ($t^* >> A^2$) BEHAVIOR AND POWER LAW REGIME: It is also evident from Figure S1 that at dimensionless times $t^* \sim A$, $h\left(t^*\right)\overline{T_a}$ becomes largely insensitive to the advective travel time distribution (i.e. α), and approaches a limiting distribution (controlled by matrix diffusion, with little dependence on the advective travel time distribution) for a given A. A late time power law regime is identified for $t^* >> A^2$, where further asymptotic expansion of

206 (S33) and (S44) produces the leading behavior shown in (S36) for any advective travel time
207 distribution, which is also verified in Figures S1 and S2.

208 $$h\left(t^*\right)\overline{T_a} \sim \frac{A}{\sqrt{\pi}t^{*3/2}} \qquad \text{(S36)}$$

209 However, this limit appears to be of limited practical value because it is only valid at very late
210 times when the influence of a finite matrix width may already be manifest.

211 IN SUMMARY: The general analytical approximations (S33) and (S34) are valid for $t^* > 1/A$,
212 and the approximate power law (S35) is valid for $1/A < t^* < 4A^2/\alpha^2$, when the values of A and
213 α are such that this time regime exists. For finite matrix widths, the influence of a finite matrix
214 is not experienced for $t^* < B^2/\left(D_e\overline{T}_a\right)$. Thus, the power law regime (S35) is valid even for
215 finite matrix widths, in the dimensionless time range $1/A < t^* < \min(B^2/\left(D_e\overline{T}_a\right), 4A^2/\alpha^2)$.
216 This behavior is evident in Figures 2b and 3b in the main manuscript, where the infinite and
217 finite matrix width cases follow the same solute TTD for a significant time range. At $t^* \sim A$,
218 $h\left(t^*\right)\overline{T_a}$ becomes largely insensitive to the advective travel time distribution (i.e. α), and
219 approaches a limiting distribution that only depends on A.

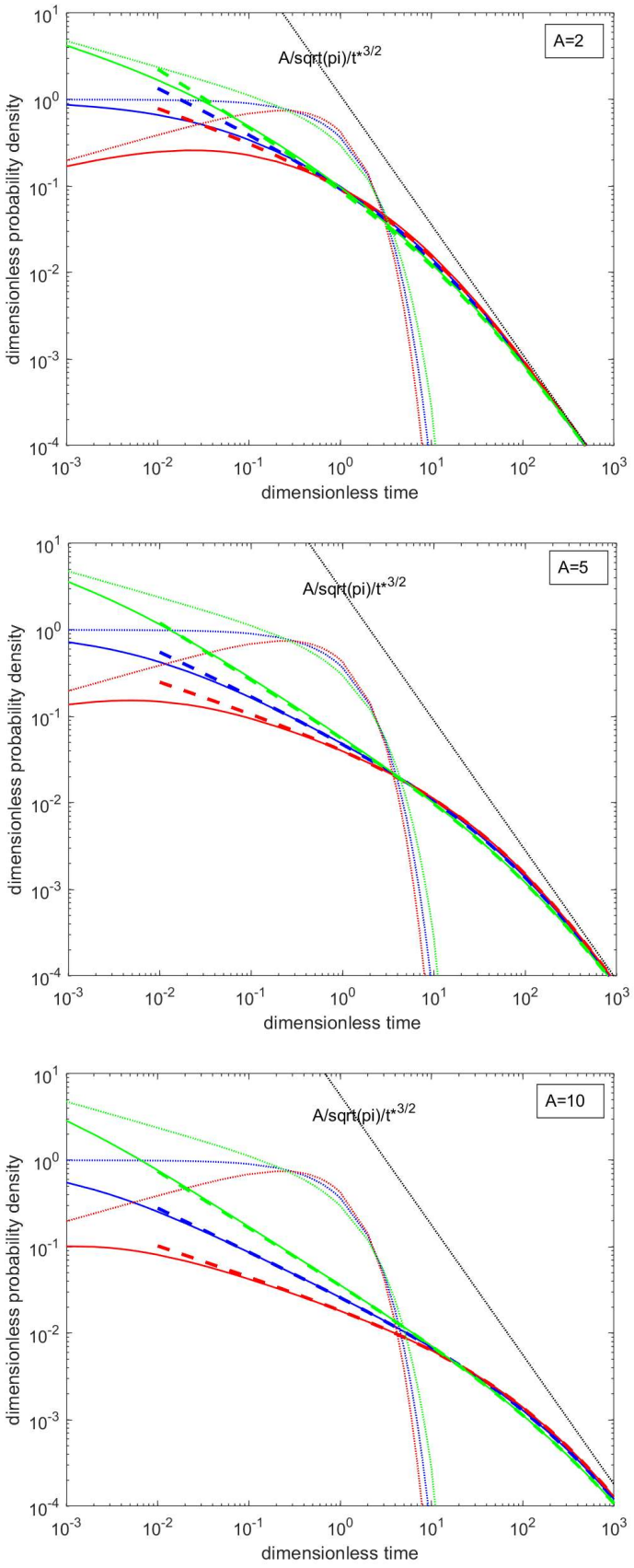

Figure S1. Dimensionless solute TTD $h\left(t^*\right)\overline{T_a}$ versus dimensionless time (t^*) for infinite matrix widths and different values of A, for gamma distributions with $\alpha = 0.7$ (green), 1 (blue) and 1.3 (red). Note that α =1 corresponds to the exponential distribution. Dotted lines: Dimensionless advective travel time distributions $P\left(T_a^*\right)\overline{T_a}$, Solid lines - Exact $h\left(t^*\right)\overline{T_a}$ from numerical integration of (S30), Dashed lines – Approximations (S33) and (S34). The straight line representing the late-time asymptote $h\left(t^*\right)\overline{T_a} \to A/\left(\sqrt{\pi}t^{*3/2}\right)$ (S36) is also shown.

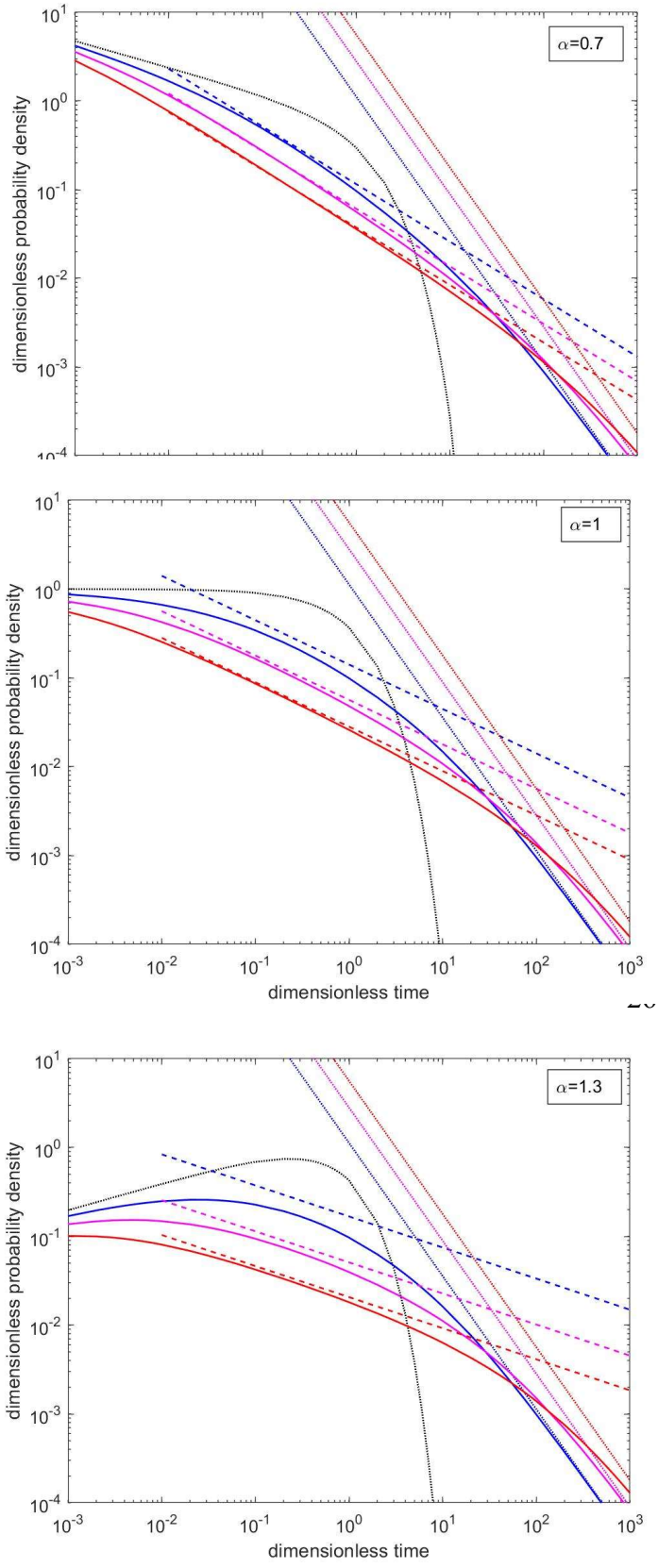

Figure S2. Dimensionless solute TTD $h\left(t^*\right)\overline{T_a}$ versus dimensionless time (t^*) for infinite matrix widths and gamma distributions with different values of α. For each value of α, the behavior is shown for different values of A, $A = 2$ (blue), 5 (magenta) and 10 (red). The dotted black line in each plot shows the advective travel time distributions $P\left(T_a^*\right)\overline{T_a}$ for the corresponding α.
Solid lines - Exact $h\left(t^*\right)\overline{T_a}$ from numerical integration of (S30),
Dashed lines – intermediate-time power-law approximation from (S35)
Dotted lines – very late time asymptote $h\left(t^*\right)\overline{T_a} \to A/\left(\sqrt{\pi}t^{*3/2}\right)$ (S36)

S.5 Stream Concentration Power Spectra Obtained with Alternative Parameter Sets for Lower Hafren

As noted in the main body of the paper, the power spectral ratio $S_{C_oC_o} / S_{C_iC_i}$ depends on two parameters, the mean advective travel time $\overline{T}_a$ and the matrix diffusion parameter A. The dimensionless parameter A involves products and ratios of other physical parameters. I present calculations of $S_{C_oC_o} / S_{C_iC_i}$ for two additional sets of parameters below. The rationale for these additional sets was simply that I used values of $\overline{T}_a$ = 0.5 and 2 times the value in the base case included in the main manuscript, and refitted other parameters to match the estimated stream concentration power spectrum in Figure (3a). The parameter values are shown in Table S.1.

	$\overline{T}_a$ (years)	ϕ_m	D_e (m^2/s)	b (m)	A
Base Case	0.01	0.15	1.5e-10	5e-4	2.06
Half $\overline{T}_a$	0.005	0.1	1.5e-10	2e-4	2.43
Double $\overline{T}_a$	0.02	0.05	1.5e-10	5e-4	0.97

Table S1. Alternative Parameter Combinations

Figure S3 shows the power spectra obtained with parameters in the second and third rows of Table S1. The "Half $\overline{T}_a$"parameter set produces an acceptable fit and improves the match to sample spectra at higher frequencies. The "Double $\overline{T}_a$" parameter set produces an acceptable fit with a larger mismatch compared to the base case at frequencies > 10^2 year^{-1}. The non-uniqueness involved in the estimating catchment-scale matrix diffusion parameters is acknowledged. However, the fitted parameter values are within acceptable ranges for these parameters. Figure S4 shows the power spectra obtained with the base case parameters and the alternative precipitation concentration power spectrum $0.38/f^{0.34}$ (mg/L)^2-yr.

(a)

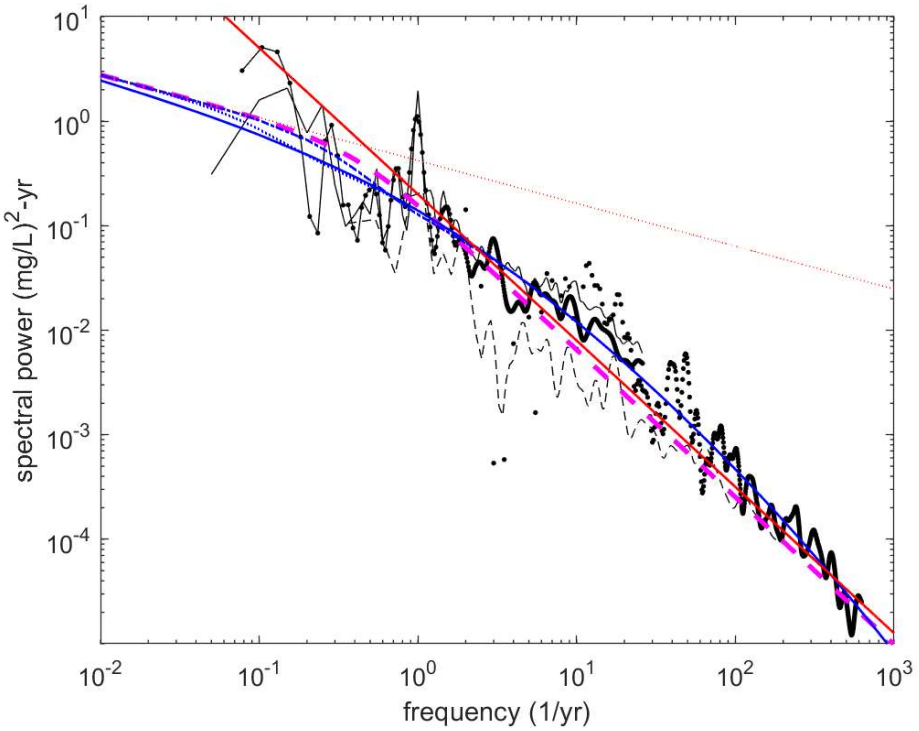

(b)

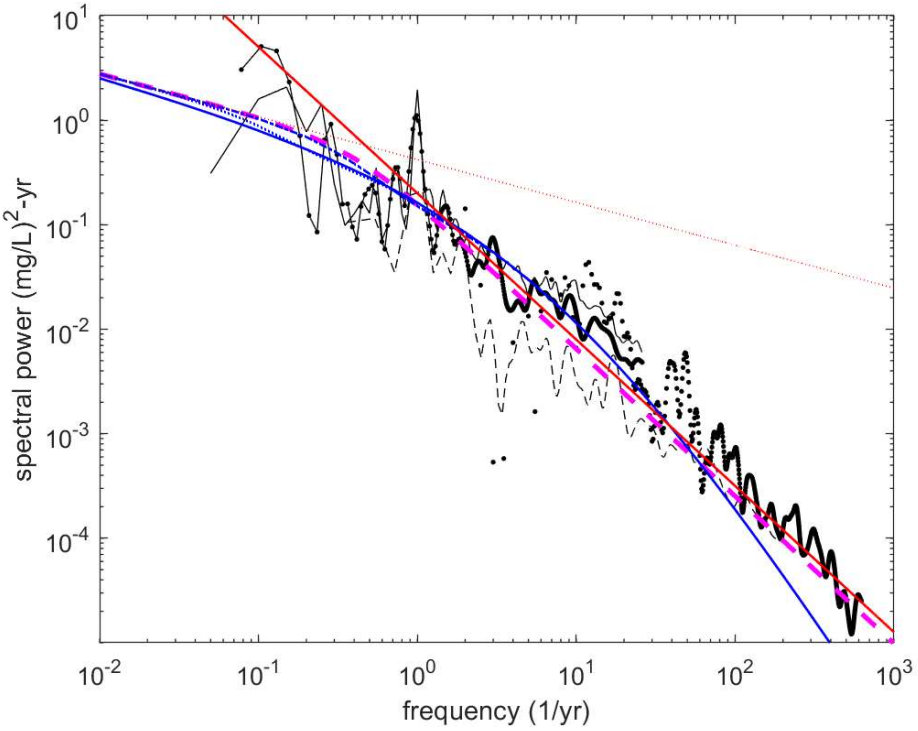

Figure S3. Stream (concentration power spectra calculated using alternative parameter sets shown in Table S1. (a) Half $\overline{T}_a$ and (b) Double $\overline{T}_a$, compared to $\overline{T}_a$ in the base case (Figure 3a in the main body of the paper). Color schemes are same as in Figure 3a. Black symbols and lines represent spectral estimates from Kirchner et al. (2013), magenta dashed line is the power spectrum corresponding to a gamma distribution ($\alpha = 0.5,\ \beta = 0.4\text{yr}$), blue lines are power spectra obtained from the matrix diffusion model (solid – infinite matrix, dashed – B = 0.1m,

dash-dotted – B = 0.05m), the red solid line indicates a spectral slope of -1.4, and the red dotted line shows the precipitation concentration spectrum.

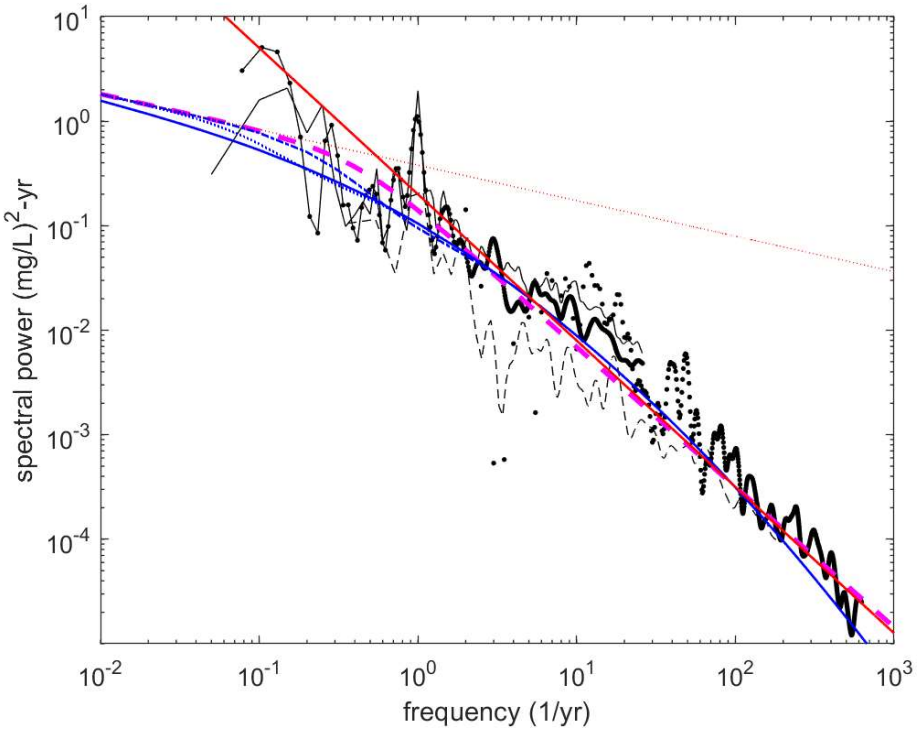

Figure S4. Stream concentration power spectra calculated using alternative precipitation chloride power spectrum $S_{C_iC_i}(f) = 0.38 / f^{0.34}$. Compared to Figure 3a, the differences are minor. Color schemes are same as in Figure 3a. Black symbols and lines represent spectral estimates from Kirchner et al. (2013), magenta dashed line is the power spectrum corresponding to a gamma distribution ($\alpha = 0.5$, $\beta = 0.4\,\mathrm{yr}$), blue lines are power spectra obtained from the matrix diffusion model (solid – infinite matrix, dashed – B = 0.1m, dash-dotted – B = 0.05m), the red solid line indicates a spectral slope of -1.4, and the red dotted line indicates the precipitation concentration spectrum.